

MIT Open Access Articles

*Brush#First ROMP of poly(ethylene oxide)
macromonomers of varied length: impact of polymer
architecture on thermal behavior and Li + conductivity*

The MIT Faculty has made this article openly available. **Please share**
how this access benefits you. Your story matters.

Citation: Shibuya, Yoshiki, Tatara, Ryoichi, Jiang, Yivan, Shao#Horn, Yang and Johnson, Jeremiah A. 2018. "Brush#First ROMP of poly(ethylene oxide) macromonomers of varied length: impact of polymer architecture on thermal behavior and Li + conductivity." Journal of Polymer Science Part A: Polymer Chemistry, 57 (3).

As Published: <http://dx.doi.org/10.1002/pola.29242>

Publisher: Wiley

Persistent URL: <https://hdl.handle.net/1721.1/140851>

Version: Author's final manuscript: final author's manuscript post peer review, without publisher's formatting or copy editing

Terms of use: Creative Commons Attribution-Noncommercial-Share Alike



Johnson Jeremiah A. (Orcid ID: 0000-0001-9157-6491)

/

Brush-First ROMP of Poly(ethylene oxide) Macromonomers of Varied Length: Impact of Polymer Architecture on Thermal Behavior and Li⁺ Conductivity

This manuscript is dedicated to Professor Mitsuo Sawamoto for his life-long outstanding achievements in polymer chemistry.

Yoshiki Shibuya,^{1*} Ryoichi Tatara,^{2*} Yivan Jiang,¹ Yang Shao-Horn,^{2,3,4} Jeremiah A. Johnson¹

¹Department of Chemistry, Massachusetts Institute of Technology, Cambridge, Massachusetts 02139, United States

²Research Laboratory of Electronics, Massachusetts Institute of Technology, Cambridge, Massachusetts 02139, United States

³Department of Mechanical Engineering, Massachusetts Institute of Technology, Cambridge, Massachusetts 02139, United States

⁴Department of Materials Science and Engineering, Massachusetts Institute of Technology, Cambridge, Massachusetts 02139, United States

Correspondence to: Jeremiah A. Johnson (E-mail: jaj2109@mit.edu)

*These authors contributed equally to this article.

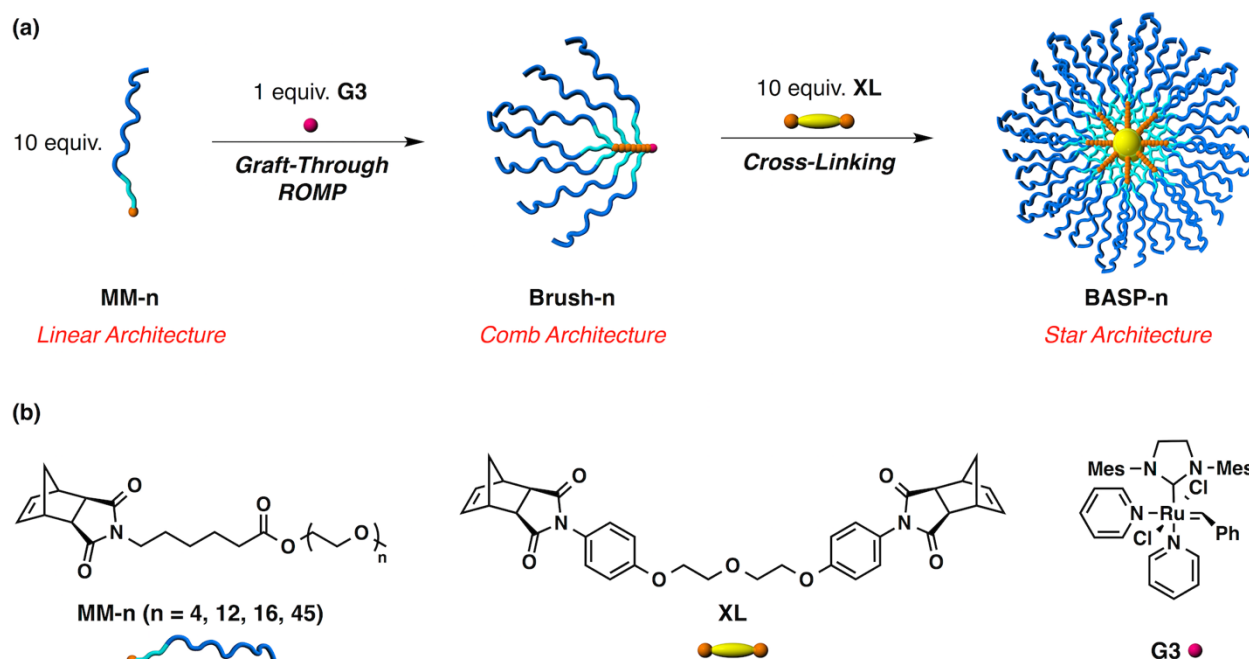
((Additional Supporting Information may be found in the online version of this article.))

ABSTRACT: The properties of polymeric materials are dictated not only by their composition but also by their molecular architecture. Here, by employing brush-first ring-opening metathesis polymerization (ROMP), norbornene-terminated poly(ethylene oxide) (PEO) macromonomers (**MM-n**, linear architecture), bottlebrush polymers (**Brush-n**, comb architecture), and brush-arm star polymers (**BASP-n**, star architecture), where **n** indicates the average degree of polymerization (DP) of PEO, are synthesized. The impact of architecture on the thermal properties and Li⁺ conductivities for this series of PEO architectures is investigated. Notably, in polymers bearing PEO with the highest degree of polymerization, irrespective of differences in architecture (linear versus star structures) and molecular weights (~100 fold differences), electrolytes with lithium bis(trifluoromethanesulfonyl)imide (LiTFSI) as a Li⁺ source exhibit normalized ionic conductivities (σ_n) within only 4.9 times difference ($\sigma_n = 29.8 \times 10^{-5} \text{ S cm}^{-1}$ for **MM-45** and $\sigma_n = 6.07 \times 10^{-5} \text{ S cm}^{-1}$ for **BASP-45**) at a concentration of Li⁺ ($r = [\text{Li}^+]/[\text{EO}] = 1/12$) at 50 °C.

KEYWORDS: macromonomer, bottlebrush polymer, brush-arm star polymer (BASP), ring-opening metathesis polymerization (ROMP), poly(ethylene oxide), electrolyte, lithium-ion battery

INTRODUCTION In order to address the safety and mechanical stability issues of liquid electrolytes in lithium-ion batteries, solid polymer electrolytes have been extensively

This is the author manuscript accepted for publication and has undergone full peer review but has not been through the copyediting, typesetting, pagination and proofreading process, which may lead to differences between this version and the Version of Record. Please cite this article as doi: [10.1002/pola.29242](https://doi.org/10.1002/pola.29242)



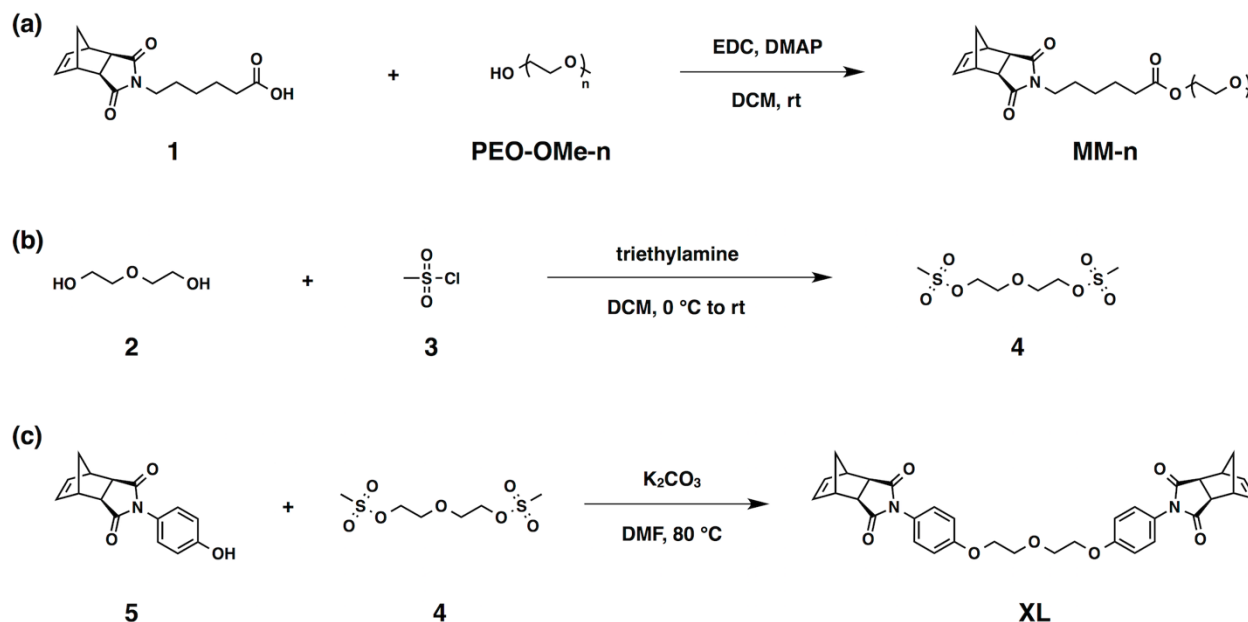
investigated.^{1–4} Poly(ethylene oxide) (PEO) is the most widely used polymer electrolyte because of its high affinity for Li^+ and low glass transition temperature (T_g).^{5–8} While PEO exhibits high ionic conductivity ($> 10^{-4} \text{ S cm}^{-1}$) above 70°C , the conductivity dramatically decreases to $\sim 10^{-7} \text{ S cm}^{-1}$ at room temperature

due to the formation of crystalline domains.⁸ It is well known that segmental motion facilitates the migration of Li^+ ions through amorphous PEO domains;⁸ analogous motion is hindered in crystalline regions. Accordingly, one strategy to improve the ionic conductivity of PEO at lower temperatures involves inhibition of

FIGURE 1 (a) Schematic illustration of “brush-first” ROMP. (b) Chemical structures of macromonomers (**MM-n**), cross-linker (**XL**), and Grubbs third-generation catalyst (**G3**).

crystallization via the use of non-linear polymer architectures such as comb-like architectures (grafted or bottlebrush polymers),^{9–13} star polymers, or dendrimers;^{14–18} however, to our knowledge, there have been no systematic comparisons of how ionic conductivity and thermal behavior vary for architectural changes from linear to comb to stars derived from the same components. To do so would require a synthetic approach to provide those three polymeric architectures from *the same* set of precursors.

We have developed brush-first ring-opening metathesis polymerization (ROMP) for the synthesis of brush-arm star polymers (BASPs).^{19–26} In this method, linear norbornene-terminated macromonomers are polymerized to produce living bottlebrush polymers. Subsequent addition of a bis-norbornene cross-links these bottlebrush polymers to yield BASPs. Brush-first ROMP allows one to easily tune the molecular weight of BASPs by changing the amount of cross-linker added and the brush degree of polymerization.¹⁹ Notably, the process of “brush-first” ROMP involves linear starting materials



(macromonomers), proceeds through a bottlebrush intermediate, and ends with BASPs. Thus, this system provides an ideal model to investigate how transitions in molecular architecture impact the bulk thermal properties and ionic conductivity of PEO-based materials.

Herein, we prepare macromonomers (**MM-n**), bottlebrush polymers (**Brush-n**), and BASPs (**BASP-n**), where **n** indicates the average degree of polymerization (DP) of PEO, all appearing in the “brush-first” synthesis (Fig. 1a). PEO-based materials featuring four different **n** values (**n** = 4, 12, 16, 45) were prepared. Bulk-state properties such as thermal behavior and ionic conductivity

of electrolytes composed of those polymers and lithium bis(trifluoromethanesulfonyl)imide (LiTFSI) are investigated. Our results shed light on the impact of different polymer architectures (linear, comb, and star architectures; Fig. 1a) on these bulk-state properties.

EXPERIMENTAL

General

All reagents and solvents were purchased from commercial suppliers and used as supplied unless otherwise noted. Norbornene-carboxylic acid imide (**1**),¹³ norbornene-phenol (**5**),²² PEO

SCHEME 1 Synthesis of macromonomers (**MM-n**) and cross-linker (**XL**).

macromonomers (**MM-12**, **MM-16**, **MM-45**),¹³ and ruthenium initiator (**G3**)²⁷ were prepared according to literature procedures. For the syntheses of PEO macromonomers (**MM-12**, **MM-16**, **MM-45**), PEO monomethyl ether (average M_n = 550 (**PEO-OMe-12**), 750 (**PEO-OMe-16**), and 2000 g/mol (**PEO-OMe-45**)) from Sigma Aldrich were used, respectively. ¹H nuclear magnetic

resonance (¹H-NMR) and ¹³C nuclear magnetic resonance (¹³C-NMR) spectra were recorded on a JEOL JNM-ECZ500R spectrometer operating at 500 and 126 MHz for ¹H and ¹³C NMR, respectively, where the chemical shifts were determined with respect to CHCl₃ (δ 7.26 ppm) or CH₂Cl₂ (δ 5.32 ppm) for ¹H NMR spectroscopy and CDCl₃ (δ 77.0 ppm) for ¹³C NMR spectroscopy as

internal standards, and splitting patterns are designated as s (singlet), d (doublet), t (triplet), and m (multiplet). Coupling constants J are reported in Hertz (Hz). Delta NMR software was used to analyze the NMR spectra. MALDI-TOF mass spectrometry was conducted by a Bruker model MicroFlex instrument using α -cyano-4-hydroxycinnamic acid (CCA) as a matrix. High-resolution mass spectra (HRMS) were obtained using a Bruker Daltonics APEXIV 4.7 Tesla Fourier Transform Ion Cyclotron Resonance Mass Spectrometer (FT-ICR-MS). Gel permeation chromatography (GPC) was performed using two Agilent PLgel 5 μ m MIXED-C 300 \times 7.5 mm columns connected in series with a DAWN EOS 18 angle laser light scattering (MALLS) detector (Wyatt Technology) and a T-rEX refractive index detector (Wyatt Technology). Experiments were performed at 60 °C using 0.025 M LiBr in *N,N*-dimethylformamide (DMF) eluent at a flow rate of 1 mL / min. The refractive index increment (dn/dc) was measured for **MM-n** and **BASP-n**. Molecular weights and dispersities were determined from the dn/dc values that were obtained assuming 100% mass elution from the columns. Dialysis tubing of cellulose ester with a MWCO of 6–8 kD was purchased from Spectrum Laboratories, Inc. Before use, the tubing was washed with deionized water. Differential scanning calorimetry (DSC) was performed on a TA Instruments Discovery DSC. Thermogravimetric analysis (TGA) was performed on a TA Instruments Discovery TGA.

Synthesis of MM-4

A dichloromethane (DCM) solution (150 mL) of *N*-(3-dimethylaminopropyl)-*N'*-ethylcarbodiimide hydrochloride (EDC, 9.72 g, 50.7 mmol), 4-(dimethylamino)pyridine (DMAP, 387 mg, 3.19 mmol), norbornene-carboxylic acid imide (**1**)¹³ (10.6 g, 38.2 mmol) and tetraethylene glycol monomethyl ether (**PEO-OMe-4**) (6.60 g, 31.7

mmol) was stirred for 22 hours at 25 °C under N₂ atmosphere. Then, the mixture was washed three times with 1 M HCl and once with brine. The organic extract was dried over anhydrous Na₂SO₄, and evaporated to dryness. The residue was chromatographed on silica gel with hexane/AcOEt (1/6) as an eluent, where the main fraction was collected and evaporated to dryness, affording **MM-4** as colorless liquid in 63% yield (9.38 g, 20.1 mmol). ¹H NMR (500 MHz, CDCl₃, 25 °C) δ (ppm) 6.24 (m, 2H), 4.17 (d, J = 4.8 Hz, 2H), 3.65 (t, J = 5.0 Hz, 2H), 3.62–3.59 (m, 10H), 3.51–3.50 (m, 2H), 3.41 (t, J = 7.5 Hz, 2H), 3.33 (s, 3H), 3.23 (s, 2H), 2.63 (m, 2H), 2.28 (t, J = 7.5 Hz, 2H), 1.60 (m, 2H), 1.52 (m, 2H), 1.47 (d, J = 10 Hz, 1H), 1.28 (m, 2H), 1.17 (d, J = 10 Hz, 1H); ¹³C NMR (126 MHz, CDCl₃, 25 °C) δ (ppm) 177.7, 173.0, 137.5, 71.6, 70.3, 70.2, 70.2, 68.8, 63.1, 58.7, 47.5, 44.8, 42.4, 38.1, 33.5, 27.1, 26.1, 24.0; HRMS-ESI m/z calcd. for C₂₄H₃₇NO₈ [M+NH₄]⁺ 485.2857, found 485.2863.

Synthesis of 4

To a DCM solution (140 mL) of diethylene glycol (**2**) (10.0 g, 94.2 mmol) and triethylamine (32.8 mL, 236 mmol) was added methanesulfonyl chloride (**3**) (18.2 mL, 236 mmol) dropwise at 0 °C under N₂ atmosphere. After being warmed to 25 °C, the reaction mixture was stirred for 20 hours. Then, 1 M HCl was added to the mixture. The resulting mixture was extracted with DCM, and the lower and upper phases separated were collected, respectively. Then, DCM was added to the aqueous extract. The resulting mixture was extracted three times with DCM. The combined organic extracts were washed with brine, dried over anhydrous Na₂SO₄, and evaporated to dryness, affording **4** as an orange powder (24.1 g), which was used for the next step without further purification.

Synthesis of XL

A DMF solution (25 mL) of norbornene-phenol (**5**)²² (854 mg, 3.35 mmol), crude **4** (399 mg, 1.52 mmol), and K₂CO₃ (1.26 g, 9.12 mmol) was stirred for 24 hours at 80 °C under N₂ atmosphere. Then, the reaction mixture was poured into an ice/water mixture. The resulting mixture was extracted with DCM. The organic extract was washed with brine, dried over with Na₂SO₄, and evaporated to dryness. The residue was chromatographed on silica gel with hexane/AcOEt (1/3) as an eluent, where the main fraction was collected and evaporated to dryness, affording **XL** as white powder in 56% yield (490 mg, 0.844 mmol). ¹H NMR (500 MHz, CDCl₃, 25 °C) δ (ppm) 7.17–7.14 (m, 4H), 7.00–6.97 (m, 4H), 6.34 (t, *J* = 1.8 Hz, 4H), 4.16 (t, *J* = 4.8 Hz, 4H), 3.92 (t, *J* = 4.8 Hz, 4H), 3.39 (t, *J* = 1.5 Hz, 4H), 2.83 (d, *J* = 1.0 Hz, 4H), 1.60 (d, *J* = 10 Hz, 2H), 1.47 (d, *J* = 10 Hz, 2H); ¹³C NMR (126 MHz, CDCl₃, 25 °C) δ (ppm) 177.3, 158.6, 137.9, 127.5, 124.7, 115.2, 69.8, 67.7, 47.8, 45.7, 42.9; HRMS-ESI *m/z* calcd. for C₃₄H₃₂N₂O₇ [M+NH₄]⁺ 598.2548, found 598.2551.

General Brush-n Synthesis via ROMP

Brush syntheses were performed in a glovebox.

MM-n was added to a vial containing a stir bar. DCM was added to the vial with **MM-n** followed by a freshly prepared solution of **G3** in DCM (7 mg **G3**/ mL DCM, amount added to give desired **MM-n:G3** (10:1)) such that the total concentration of **MM-n** was 0.04 M. The reaction mixture was allowed to stir for 90 min at 25 °C, at which point excess ethyl vinyl ether (EVE) was added to quench the polymerization. The resulting mixture was subjected to reprecipitation in diethyl ether at –78 °C. The precipitates were collected and dried under reduced pressure, affording **Brush-n** as a powder or viscous liquid.

General BASP-n Synthesis via ROMP

BASP syntheses were performed in a glovebox. **MM-n** was added to a vial containing a stir bar. 10 equivalents of **XL** were added to a separate vial containing stir bar. THF was added to the vial with **MM-n** followed by a freshly prepared solution of **G3** in THF (7 mg **G3**/ mL THF, amount added to give desired **MM-n:G3** (10:1)) such that the total concentration of **MM-n** was 0.04 M. The reaction mixture was allowed to stir for 20 min at 25 °C before an aliquot (~5 µL) was taken out and quenched with 1 drop of EVE for GPC analysis. Then, the reaction mixture was transferred to the vial containing **XL**. The resulting mixture was stirred for 7 hours at 25 °C, at which point excess EVE was added to quench the polymerization. The quenched mixture was transferred to a 6–8 kD molecular weight cutoff dialysis tubing containing nanopure water, and the solution was dialyzed against water (3 times, solvent exchange every 6 hours).²⁸ The resulting mixture was then lyophilized, affording **BASP-n** as a powder.

Preparation of Electrolytes

Polymer and LiTFSI were dissolved in acetonitrile in a 4 mL vial. Most of the acetonitrile was evaporated in a fume hood overnight. The resulting sample was further dried at 100 °C under reduced pressure for at least 6 hours, affording an electrolyte for ionic conductivity measurement.

Ionic Conductivity Measurement

Ionic conductivity was measured using the complex impedance method, using two stainless steel plates as blocking electrode, in the frequency range from 1 MHz to 500 mHz with 100 mV sinusoidal amplitude by using a VMP3 (Bio-Logic) potentiostat. Fluid electrolytes (from **PEO-OMe-45**, **MM-4**, **MM-12**, **MM-16**, **MM-45**, **Brush-4**, **Brush-12**, **Brush-16**, **Brush-45**, and **BASP-45** as a polymer) were directly transferred to a stainless-steel plate with a Teflon spacer (I.D.

= 3.6 mm ϕ , thickness = 1.6 mm). Non-fluid electrolytes (from **BASP-4**, **BASP-12**, and **BASP-16**) were first pelletized with a hydraulic press and dies (6 mm ϕ), and then free-standing pelletized samples were sandwiched with two stainless-steel plates (thickness of the pelletized samples were measured after conductivity measurement). The cell was thermally equilibrated at each temperature for 1 hour using a thermostat chamber (SU-241, Espec) before conductivity was measured.

RESULTS AND DISCUSSION

We began with the synthesis of PEO macromonomers (**MM-n**, Fig. 1b) from norbornene-carboxylic acid imide (**1**)¹³ (Scheme 1) and PEO monomethyl ether (**PEO-OMe-n**) according to a reported procedure.¹³ Grubbs third-generation bis-pyridine catalyst²⁷ (**G3**, Fig. 1b) was used as the initiator for all ROMP reactions. The cross-linker (**XL**, Fig. 1b) for the formation of BASPs (**BASP-n**, Fig. 1a) was synthesized from norbornene-phenol (**5**)²² (Scheme 1) and bis-mesylated diethylene glycol (**4**) (Scheme 1) via Williamson-etherification. Full synthetic details are provided in the experimental section. These molecules were characterized by ¹H and ¹³C NMR spectra, high-resolution mass spectra (ESI), and MALDI-TOF mass spectrometry (Figs. S20–S26, S35–S38 in the supporting information). The gel-permeation chromatography (GPC) refractive index traces for **MM-n** (**n** = 12, 16, 45) are provided in Fig. S1 (see supporting information) and the characterization data are summarized in Table 1.

Brush-n samples were synthesized from corresponding **MM-n** via ROMP. **MM-n** (10 equiv)

TABLE 1 Physical characterization of polymers synthesized in this study.

were exposed to **G3** (1 equiv) in DCM for 90 min to form bottlebrush polymers **Brush-n** with a DP of 10 (Fig. 1a). Full synthetic details are provided in the experimental section. The GPC traces of **Brush-n** are provided in Fig. S2 and the molecular weight data are shown in Table 1.

Brush-first ROMP was employed for the syntheses of **BASP-n** (Fig. 1a). First, **MM-n** (10 equiv) were exposed to **G3** (1 equiv) in THF for 20 min to form bottlebrush polymers with a number-average DP of 10. Then, without quenching the reaction, the living bottlebrush polymer solution was added to a vial containing 10 equiv of **XL** (Fig. 1b). After 7 h, the polymerization reaction was quenched with excess ethyl vinyl ether. The resulting mixture was dialyzed against water, and was subsequently subjected to lyophilization, affording **BASP-n**. The synthesized **BASP-n** displayed monomodal GPC traces (Fig. S3). The number-average molar mass (M_n , Table 1) of **BASP-n** (Fig. S3) varied inversely with the PEO length (**n**). **BASP-4** had a much broader dispersity (M_w/M_n , Table 1) than that of other BASPs. These results indicate that bottlebrush polymers with shorter PEO sidechains can more efficiently cross-link with each other, and eventually over cross-link leading to lack of control, due to limited steric hindrance around the BASP core. This same uncontrolled arm-first crosslinking of small monomers motivated our development of brush-first ROMP.¹⁹

The thermal behavior of **MM-n**, **Brush-n**, and **BASP-n** were investigated. As a reference, physical

MM-n

Polymer	M_n (kg/mol) ^a	M_w/M_n ^b	n ^c	T_g (°C) ^d	T_c (°C) ^d	T_m (°C) ^d
MM-4	—	— ^e	4	−65	n.d.	n.d.
MM-12	0.801	— ^e	12	n.d.	−44	11
MM-16	0.990	— ^e	16	n.d.	n.d.	30
MM-45	2.37	1.08	45	n.d.	n.d.	50

Brush-n

Polymer	DP _{theo}	M_n (kg/mol) ^a	DP _{exp} ^a	M_w/M_n ^b	T_g (°C) ^d	T_c (°C) ^d	T_m (°C) ^d
Brush-4	10	4.67	10	1.11	−49	n.d.	n.d.
Brush-12	10	7.21	9	1.03	n.d.	−21	11
Brush-16	10	7.92	8	1.18	n.d.	n.d.	32
Brush-45	10	21.3	9	1.15	n.d.	n.d.	50

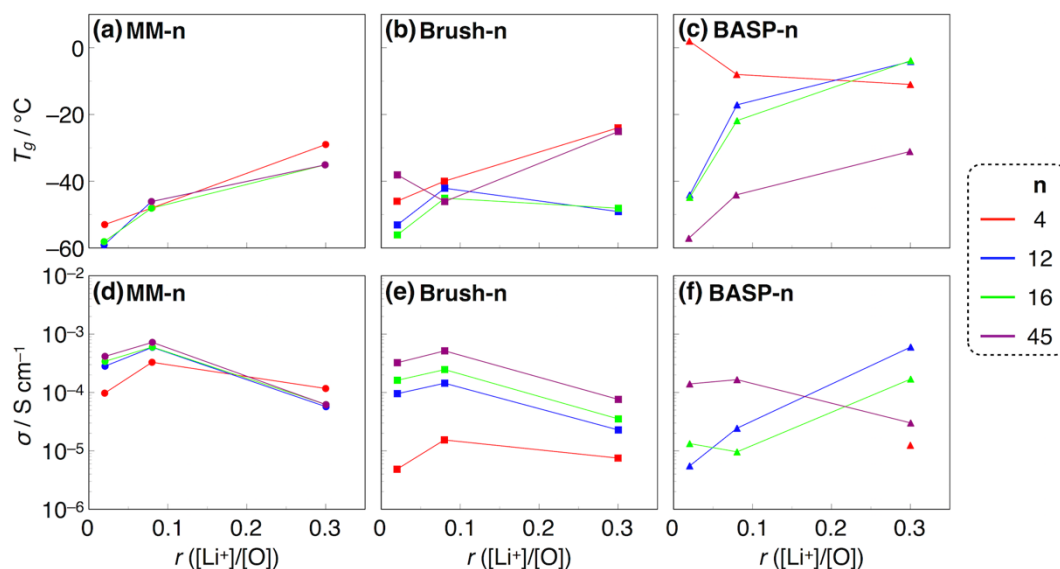
BASP-n

Polymer	DP _{brush, theo} ^f	M_n (kg/mol) ^b	M_w/M_n ^b	T_g (°C) ^d	T_c (°C) ^d	T_m (°C) ^d
BASP-4	10	2260	1.77	1	n.d.	n.d.
BASP-12	10	627	1.15	32	n.d.	n.d.
BASP-16	10	254	1.36	30	n.d.	n.d.
BASP-45	10	240	1.13	n.d.	n.d.	50

^a Determined by ¹H NMR. ^b Determined by GPC-MALLS. ^c Reported by supplier. ^d Detected in DSC traces (2nd heating cycle) at a scan rate of 10 °C/min. ^e The full peak in GPC traces did not elute prior to the end of sample run (see Fig. S1), which made it impossible to determine M_w/M_n . ^f The molar equivalent of **MM-n** against **XL** in the synthesis of **BASP-n** (see Fig. 1 and EXPERIMENTAL section). T_g : glass transition temperature. T_c : crystallization temperature. T_m : melting temperature. n.d.: not detected.

characterization of **PEO-OMe-n** used for the syntheses of **MM-n** are provided in Figs. S8–S10, and Table S1. First, the thermal stability of the polymers was studied by thermogravimetric analysis (TGA). While **MM-n** samples decomposed (corresponding to 5 wt% loss) at a temperature range of 251 °C–277 °C (Fig. S4),

Brush-n and **BASP-n** were thermally stable up to a temperature range of 349 °C–371 °C (Figs. S5 and S6). The TGA thermograms clarify that electrolytes prepared from these polymers can be used in a wide operating temperature without degradation. Next, we investigated the phase behavior of these polymers by differential



scanning calorimetry (DSC). DSC traces and the summary of glass transition temperature (T_g), crystallization temperature (T_c), and melting temperature (T_m) on heating are shown in Fig. S7

FIGURE 2 Glass transition temperatures (T_g) (a–c) and ionic conductivities at 70 °C (d–f) of electrolytes composed of polymers and LiTFSI at various concentrations ($r = 0.02, 0.08$, and 0.3). Ionic conductivity data of electrolytes prepared from **BASP-4** at $r = 0.02$ and 0.08 are not shown in (f) because of quite low values (the order of $10^{-7} \text{ S cm}^{-1}$).

4, samples with the same DP show similar melting temperature (Tables 1 and S1), indicating that if the PEO length is sufficient, the effect of the norbornene-containing chain end is negligible. Polymers having the shortest PEO length ($n = 4$) exhibited only glass transitions without melting behavior. The glass transition temperature (T_g) of **BASP-4** ($T_g = 1$ °C, Fig. S7 and Table 1) is much greater than that of **MM-4** ($T_g = -65$ °C, Fig. S7 and Table 1) and **Brush-4** ($T_g = -49$ °C, Fig. S7 and Table 1). In the cases of PEO length $n = 12$ or 16 , both macromonomers (**MM-12** or **MM-16**) and bottlebrush polymers (**Brush-12** or **Brush-16**) were semi-crystalline; there was almost no change of melting temperature (T_m) at the architectural transition from linear to comb architecture (Fig. S7 and Table 1). In contrast,

and Table 1, respectively. Comparing the thermal behavior of **PEO-OMe-n** and **MM-n**, except for $n =$

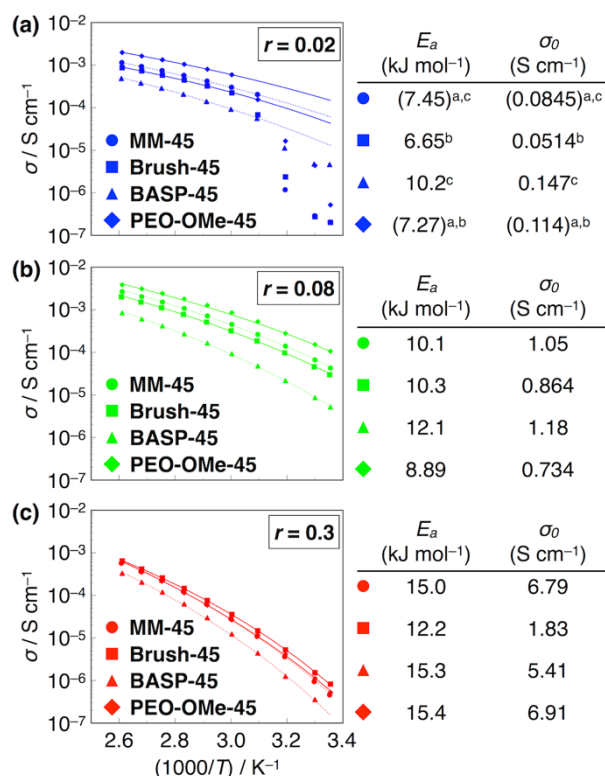
BASPs having PEO length $n = 12$ or 16 (**BASP-12** or **BASP-16**) exhibited only glass transitions at 32 °C (**BASP-12**, Fig. S7 and Table 1) and 30 °C (**BASP-16**, Fig. S7 and Table 1), respectively. Similar to the general characteristic of star polymers, the crystallization of PEO chains is inhibited in BASPs.²⁹ Polymers with the longest PEO length ($n = 45$) all exhibited melting behavior without any glass transitions irrespective of the polymer architectures (Fig. S7 and Table 1). Furthermore, their comparable T_m values (50 °C for **MM-45**, 50 °C for **Brush-45**, and 47 °C for **BASP-45**, Fig. S7 and Table 1) indicated that architectural changes do not affect the PEO crystallinity when the PEO DP is sufficiently large. Especially regarding **BASP-45**, the PEO chains at the periphery of the star architecture appear to be sufficiently flexible

compared to the chains in other **BASP-n** ($n = 4, 12, 16$; non-crystalline polymers) to form similar crystalline domains observed in **MM-45** and **Brush-45**.

With this library of polymers in hand, we prepared electrolytes via mixing the polymers with LiTFSI at varied concentrations of $r = 0.02, 0.08$, and 0.3 , where r is the molar ratio of Li^+ to EO repeating units, $[\text{Li}^+]/[\text{O}]$. DSC clarified the effect of adding lithium salt on the thermal behavior of these electrolytes. As shown in Fig. 2a–c, in most cases, T_g increased in proportion to the concentration of Li^+ (r), demonstrating that intramolecular or intermolecular coordination of Li^+ with PEO chains restricts the segmental motion. An electrolyte prepared from **Brush-45** exhibited a decreased T_g at $r = 0.08$ compared to $r = 0.02$ (Fig. 2b, purple trace), which may be due to exclusion of Li^+ from the crystalline regions of the latter sample, thereby increasing the concentration of Li^+ in amorphous regions (see DSC trace in Fig. S12).³⁰ The T_g of an electrolyte from **BASP-4** (Fig. 2c, red trace) gradually decreased in proportion to the increase of r . This behavior may be due to plasticization instead of cross-linking of PEO chains for this architecture.³¹ The ionic conductivities (σ) at 70°C were generally the highest at $r = 0.08$ for electrolytes from **MM-n** and **Brush-n** (Fig. 2d and e). This trend is quite similar to what was observed in a previous report on standard PEO³² and in our electrolytes from **PEO-OMe-45** (Fig. 3). In contrast, interestingly, electrolytes from **BASP-n** ($n = 4, 12$, and 16) exhibited the highest ionic conductivity at $r = 0.3$ (Fig. 2f, red, blue, and green traces) despite their high T_g values, while an electrolyte from **BASP-45** showed the typical trend (Fig. 2f, purple trace). These findings suggest that **BASP-n** ($n = 4, 12$, and 16) form a network of Li^+ conducting PEO domains that facilitate Li^+ mobility regardless of the high T_g .³³

When we focused on the architecture dependency on ionic conductivity (Fig. S15a–c), this trend was also observed. For every n value at $r = 0.02$ or 0.08 , BASPs showed the lowest ionic conductivity, whereas at $r = 0.3$, ionic conductivities of BASPs in the cases of smaller n values ($n = 4, 12$ and 16) at 70°C ($1.25 \times 10^{-5} \text{ S cm}^{-1}$ for **BASP-4**, $5.87 \times 10^{-4} \text{ S cm}^{-1}$ for **BASP-12**, and $1.72 \times 10^{-4} \text{ S cm}^{-1}$ for **BASP-16**) increased at the architectural transition from **Brush-n** to **BASP-n**.

In order to understand the impact of polymer architectures on ionic conductivity in detail, we measured Li^+ conductivity at various temperatures of electrolytes prepared from **PEO-OMe-45**, **MM-45**, **Brush-45**, and **BASP-45**. As shown in Fig. 3a–c, at every concentration of LiTFSI, all of the electrolytes displayed decreased ionic conductivity as operating temperature decreased. Only at $r = 0.02$ (Fig. 3a), dramatic drops in ionic conductivity were observed. These decreases are derived from the crystallization of PEO chains at 40 – 50°C (see DSC traces in Figs. S11–S13 and S16). Notably, the electrolyte from **BASP-45** at $r = 0.02$ showed less of a drop in ionic conductivity at this temperature range (Fig. 3a, triangle symbols), indicating that even at low concentration of Li salt, crystallization of PEO chains is inhibited. The ionic conductivities of electrolytes prepared from **MM-45**, **Brush-45**, or **BASP-45** and LiTFSI as a function of $1000/T$ (T : temperature in K) at various concentrations ($r = 0.02, 0.08$, and 0.3). Fitting curves to the VTF equation are shown in solid or dotted lines. The analyzed parameters in the VTF equation are in the right side of each graph.^a T_g of the electrolytes prepared from **PEO-OMe-45** and **MM-45** ($r = 0.02$) were estimated by a linear fitting of T_g as a function of r .^b Above 60°C .^c Above 50°C .



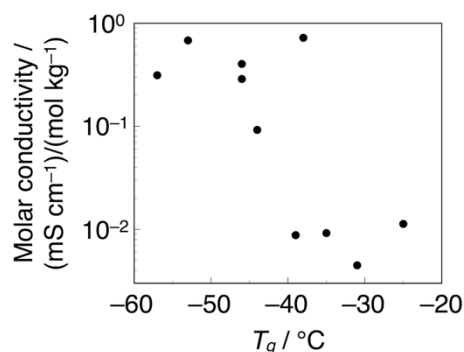
45 are comparable to those of electrolytes from **PEO-OMe-45** (Fig. 3a–c, circle and diamond symbols, respectively); the difference in ionic conductivity is within only 2.2 times above 30 °C ($\sigma = 6.75 \times 10^{-5}$ S cm⁻¹ for **MM-45** and $\sigma = 14.8 \times 10^{-5}$ S cm⁻¹ for **PEO-OMe-45** ($r = 0.08$ at 30 °C)). This trend indicates that the effect of non-conductive moiety in **MM-45** (ex. norbornene terminal) on conducting capability is quite small. The small difference in ionic conductivity above is more obvious when using the ionic conductivity divided by the mass fraction of PEO in each polymer (normalized ionic conductivity: σ_n in Figs. S14 and S15d–f for all electrolytes at 70 °C, and in Fig. S17 for all polymers with $n = 45$ at various temperatures). It is noteworthy that the normalized ionic conductivities are within only 4.9 times difference at the largest ($\sigma_n = 29.8 \times 10^{-5}$ S cm⁻¹ for **MM-45** and $\sigma_n = 6.07 \times 10^{-5}$ S cm⁻¹ for **BASP-45** ($r = 0.08$ at 50 °C)), despite the fact that

the molecular weight of **BASP-45** is ~100 times larger than that of **MM-45** (Table 1). Similar behavior has been observed for linear PEO samples of varying molecular weight.³⁴

For a further understanding of the electrolytes prepared from **PEO-OMe-45**, **MM-45**, **Brush-45**, and **BASP-45**, Vogel–Tammann–Fulcher (VTF) equation was employed.³⁵

$$\sigma(T) = \sigma_0 e^{-E_a/R(T-T_0)} \quad (1)$$

In this equation, $\sigma(T)$ is the ionic conductivity at a certain temperature, σ_0 is a constant related to the maximum number of charge carriers, E_a is the activation energy of ion conduction, R is the gas constant, T is the temperature, and T_0 is the VTF temperature often chosen to be 50 K below T_g .³⁵ The fitting curves to equation 1 in our experimental results are shown in Fig. 3a–c with solid or dotted lines. The analyzed parameters in the VTF equation are summarized in Fig. 3. As we expected, in proportion to the concentration of Li salt (r), σ_0 values increased, which indicates that even at high Li salt concentration, the salt can dissociate into Li⁺ and TFSI⁻. Interestingly, the σ_0 values of an electrolyte prepared from **BASP-45** are comparable to those of an electrolyte from **MM-45** (Fig. 3), which suggests that BASPs are capable of dissociating LiTFSI as strongly as macromonomers irrespective of their architectural differences. The activation energy (E_a) was the highest for electrolytes from **BASP-45** at every concentration of Li salt (Fig. 3). On the other hand, electrolytes from **Brush-45** showed much smaller activation energies compared to other electrolytes at all r values (Fig. 3). These results indicate that bottlebrush polymers can readily provide an efficient transportation of Li⁺ even at high concentrations of Li salt.



Imaginary impedance values for **PEO-OMe-45**, **MM-45**, **Brush-45**, and **BASP-45** with LiTFSI, **FIGURE 4** Molar conductivity of electrolytes composed of **PEO-OMe-45**, **MM-45**, **Brush-45**, or **BASP-45** and LiTFSI as a function of glass transition temperature (T_g) at various concentrations ($r = 0.02, 0.08$, and 0.3).

extracted from ionic conductivity measurements via the complex impedance method, plotted against frequency are shown in Fig. S18. Imaginary impedance represents the capacitive response of the impedance measurement, where peak frequency describes the time scale of specific processes. General and detailed assignments of imaginary impedance (or dielectric relaxation, which is directly related to imaginary impedance) behavior for polymer electrolytes are still not clear; however, the slope in the low frequency region could be assigned to ionic (DC) polarization³⁶ and the peak in the high frequency region corresponds to ion-pair relaxation or segmental relaxation of polymer chains.^{37,38} Peak top frequency for the high frequency region shows a maximum at medium concentration ($r = 0.08$) for all the electrolytes prepared from **PEO-OMe-45**, **MM-45**, **Brush-45**, and **BASP-45**. This trend is consistent with ionic conductivity trends (Figs. 2 and 3), indicating that local flexibility of ion-pairs and/or polymer chains reflected in the imaginary impedance might be a

good metric for ionic conduction in polymer electrolytes.

To further examine the effect of polymer architectures on ionic conductivity, we compared parameters measured/calculated in this work among different structures/concentrations. As shown in Fig. S19, the activation energy, glass transition temperature, peak frequency for imaginary impedance, and σ_0 values did not yield any of explicit trends. However, as shown in Fig. 4, molar conductivity decreases with increasing glass transition temperature for the electrolytes prepared from **PEO-OMe-45**, **MM-45**, **Brush-45**, and **BASP-45** with LiTFSI ($r = 0.02, 0.08$ and 0.3). Molar conductivity (Λ) was defined as $\Lambda = \sigma/c$, where c is the concentration of salt in electrolytes. Here, we used LiTFSI concentration in EO repeating unit ($\text{mol}_{\text{LiTFSI}}/\text{kg}_{\text{EO}}$) as c for each electrolyte. Generally, ionic conductivity (σ) can be described as follows:

$$\sigma = \sum_i N_i Q_i u_i \quad (2)$$

where N is charge carrier concentration, Q is charge number of ions (unity for LiTFSI) and u is mobility of ions, indicating the competing effects of charge carrier concentration and mobility of ions.³⁹ Therefore, molar conductivity, which is conductivity divided by salt concentration, can be regarded as good metric for ion mobility in the electrolyte solutions due to cancelling out of the charge carrier effect. As shown in Fig. 4, regardless of the different architectures, the electrolytes with lower glass transition temperature showed higher molar conductivity, suggesting that the glass transition temperature can be regarded as a comprehensive and global descriptor for mobility of ions among these different architectures, while activation energy (energetic barrier of ion transport), peak frequency for imaginary impedance (relaxation

time scale), and σ_0 values (maximum number of charge carrier) do not show explicit trends.

CONCLUSIONS

In conclusion, we prepared linear macromonomers (**MM-n**), bottlebrush polymers (**Brush-n**), and star-like BASPs (**BASP-n**) having various length of PEO chains. The thermal behavior of those polymers and Li^+ conductivity values of electrolytes prepared from those polymers with LiTFSI were investigated. Especially in polymers with a relatively long PEO chain ($n = 45$), irrespective of large differences in architectures and molecular weights (100 times difference between **MM-45** and **BASP-45**), the electrolytes were found to exhibit normalized ionic conductivities within only 4.9 times difference ($\sigma_n = 29.8 \times 10^{-5} \text{ S cm}^{-1}$ for **MM-45** and $\sigma_n = 6.07 \times 10^{-5} \text{ S cm}^{-1}$ for **BASP-45** ($r = 0.08$ at 50°C)). Furthermore, analyses using the VTF equation clarified that **BASP-45** has comparable capability of dissociating Li salt to **MM-45**. Finally, regardless of the polymer architecture (linear, comb, or star) the glass transition temperature was found to be a comprehensive descriptor for ion mobility. These results could contribute to the future design of nanostructured polymer electrolytes for Li-ion batteries.

ACKNOWLEDGEMENTS

We thank Mr. Graham M. Leverick for his valuable discussion. We thank the Toyota Research Institute Accelerated Materials Design and Discovery program for support of this work.

REFERENCES AND NOTES

1. W. H. Meyer, *Adv. Mater.* **1998**, *10*, 439.
2. D. T. Hallinan, N. P. Balsara, *Annu. Rev. Mater. Res.* **2013**, *43*, 503.
3. L. Long, S. Wang, M. Mao, Y. Meng, *J. Mater. Chem. A* **2016**, *4*, 10038.
4. M. A. Morris, H. An, J. L. Lutkenhaus, T. H. Epps, III, *ACS Energy Lett.* **2017**, *2*, 1919.
5. D. E. Fenton, J. M. Parker, P. V. Wright, *Polymer* **1973**, *14*, 589.
6. C. Berthier, W. Gorecki, M. Minier, M. B. Armand, J. M. Chabagno, P. Rigaud, *Solid State Ionics* **1983**, *11*, 91.
7. Z. Gadjourova, Y. G. Andreev, D. P. Tunstall, P. G. Bruce, *Nature* **2001**, *412*, 520.
8. Z. Xue, D. He, X. Xie, *J. Mater. Chem. A* **2015**, *3*, 19218.
9. A. Nishimoto, M. Watanabe, Y. Ikeda, S. Kohjiya, *Electrochim. Acta* **1998**, *43*, 1177.
10. K. Kishimoto, M. Yoshio, T. Mukai, M. Yoshizawa, H. Ohno, T. Kato, *J. Am. Chem. Soc.* **2003**, *125*, 3196.
11. J. Sun, G. M. Stone, N. P. Balsara, R. N. Zuckermann, *Macromolecules* **2012**, *45*, 5151.
12. K. P. Barteau, M. Wolffs, N. A. Lynd, G. H. Fredrickson, E. J. Kramer, C. J. Hawker, *Macromolecules* **2013**, *46*, 8988.
13. C. M. Bates, A. B. Chang, N. Momčilović, S. C. Jones, R. H. Grubbs, *Macromolecules* **2015**, *48*, 4967.
14. C. J. Hawker, F. Chu, P. J. Pomery, D. J. T. Hill, *Macromolecules* **1996**, *29*, 3831.
15. M. Marzantowicz, J. R. Dygas, F. Krok, A. Tomaszewska, Z. Florjańczyk, E. Zygadło-Monikowska, G. Lapienis, *J. Power Sources* **2009**, *194*, 51.

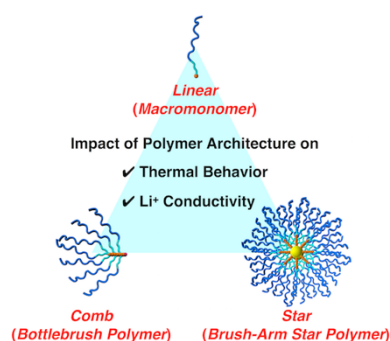
16. T. Niitani, M. Amaike, H. Nakano, K. Dokko, K. Kanamura, *J. Electrochem. Soc.* **2009**, *156*, A577.
17. D.-G. Kim, H.-S. Sohn, S.-K. Kim, A. Lee, J.-C. Lee, *J. Polym. Sci. Part A: Polym. Chem.* **2012**, *50*, 3618.
18. R. Khurana, J. L. Schaefer, L. A. Archer, G. W. Coates, *J. Am. Chem. Soc.* **2014**, *136*, 7395.
19. J. Liu, A. O. Burts, Y. Li, A. V. Zhukhovitskiy, M. F. Ottaviani, N. J. Turro, J. A. Johnson, *J. Am. Chem. Soc.* **2012**, *134*, 16337.
20. A. O. Burts, L. Liao, Y. Y. Lu, D. A. Tirrell, J. A. Johnson, *Photochem. Photobiol.* **2014**, *90*, 380.
21. L. Liao, J. Liu, E. C. Dreaden, S. W. Morton, K. E. Shopsowitz, P. T. Hammond, J. A. Johnson, *J. Am. Chem. Soc.* **2014**, *136*, 5896.
22. A. X. Gao, L. Liao, J. A. Johnson, *ACS Macro Lett.* **2014**, *3*, 854.
23. A. O. Burts, A. X. Gao, J. A. Johnson, *Macromol. Rapid Commun.* **2014**, *35*, 168.
24. J. C. Barnes, P. M. Bruno, H. V.-T. Nguyen, L. Liao, J. Liu, M. T. Hemann, J. A. Johnson, *J. Am. Chem. Soc.* **2016**, *138*, 12494.
25. H. V.-T. Nguyen, Q. Chen, J. T. Paletta, P. Harvey, Y. Jiang, H. Zhang, M. D. Boska, M. F. Ottaviani, A. Jasanoff, A. Rajca, J. A. Johnson, *ACS Cent. Sci.* **2017**, *3*, 800.
26. Y. Shibuya, H. V.-T. Nguyen, J. A. Johnson, *ACS Macro Lett.* **2017**, *6*, 963.
27. J. A. Love, J. P. Morgan, T. M. Trnka, R. H. Grubbs, *Angew. Chem. Int. Ed.* **2002**, *41*, 4035.
28. In the synthesis of **BASP-4**, precipitates appeared inside the dialysis tubing. This is because of low solubility of **BASP-4** in water. The precipitates were used for experiments without further purification.
29. G. Lapienis, *Prog. Polym. Sci.* **2009**, *34*, 852.
30. M. Marzantowicz, J. R. Dygas, F. Krok, J. L. Nowiński, A. Tomaszewska, Z. Florjańczyk, E. Zygałło-Monikowska, *J. Power Sources* **2006**, *159*, 420.
31. K. Kimura, J. Motomatsu, Y. Tominaga, *J. Phys. Chem. C* **2016**, *120*, 12385.
32. S. Lascaud, M. Perrier, A. Vallée, S. Besner, J. Prud'homme, *Macromolecules* **1994**, *27*, 7469.
33. T. Sato, T. Morinaga, S. Marukane, T. Narutomi, T. Igarashi, Y. Kawano, K. Ohno, T. Fukuda, Y. Tsujii, *Adv. Mater.* **2011**, *23*, 4868.
34. A. A. Teran, M. H. Tang, S. A. Mullin, N. P. Balsara, *Solid State Ionics* **2011**, *203*, 18.
35. M. A. Ratner, D. F. Shriver, *Chem. Rev.* **1988**, *88*, 109.
36. N. K. Karan, D. K. Pradhan, R. Thomas, B. Natesan, R. S. Katiyar, *Solid State Ionics* **2008**, *179*, 689.
37. L. R. A. K. Bandara, M. A. K. L. Dissanayake, M. Furlani, B.-E. Mellander, *Ionics* **2000**, *6*, 239.
38. F. M. Gray, C. A. Vincent, M. Kent, *J. Polym. Sci. Part B: Polym. Phys.* **1989**, *27*, 2011.
39. K. Yoshida, M. Tsuchiya, N. Tachikawa, K. Dokko, M. Watanabe, *J. Phys. Chem. C* **2011**, *115*, 18384.

GRAPHICAL ABSTRACT

Yoshiki Shibuya, Ryoichi Tatara, Yivan Jiang, Yang Shao-Horn, Jeremiah A. Johnson

Brush-First ROMP of Poly(ethylene oxide) Macromonomers of Varied Length: Impact of Polymer Architecture on Thermal Behavior and Li^+ Conductivity

Brush-first ring-opening metathesis polymerization (ROMP) provides norbornene-terminated macromonomers (linear architecture), bottlebrush polymers (comb architecture), and brush-arm star polymers (BASPs) (star architecture) with varied lengths of poly(ethylene oxide) (PEO) chains. The impact of those distinct PEO architectures on thermal property and Li^+ conductivity is investigated. Importantly, these polymers with varied architectures are derived from same components.



GRAPHICAL ABSTRACT

Yoshiki Shibuya, Ryoichi Tatara, Yivan Jiang, Yang Shao-Horn, Jeremiah A. Johnson

Brush-First ROMP of Poly(ethylene oxide) Macromonomers of Varied Length: Impact of Polymer Architecture on Thermal Behavior and Li^+ Conductivity

Brush-first ring-opening metathesis polymerization (ROMP) provides norbornene-terminated macromonomers (linear architecture), bottlebrush polymers (comb architecture), and brush-arm star polymers (BASPs) (star architecture) with varied lengths of poly(ethylene oxide) (PEO) chains. The impact of those distinct PEO architectures on thermal property and Li^+ conductivity is investigated. Importantly, these polymers with varied architectures are derived from same components.

